# Quantitative LVEF and Qualitative Regional Function from Gated Thallium-201 Perfusion SPECT

Guido Germano, Jacob Erel, Hosen Kiat, Paul B. Kavanagh and Daniel S. Berman

*Department of Medical Physics and Imaging, Division of Nuclear Medicine, Department of Imaging, and Division of Cardiology, Department of Medicine, Cedars-Sinai Research Institute, Cedars-Sinai Medical Center, Los Angeles; Departments of Radiological Sciences and Medicine, University of California at Los Angeles School of Medicine, Los Angeles, California*

This study investigates the feasibility of routine clinical $^{201}$Tl gated perfusion SPECT (gated Tl), and compares quantitative left ventricular ejection fraction (LVEF) and visually-assessed regional wall motion and thickening to analogous values obtained from $^{99m}$Tc-sestamibi gated perfusion SPECT (gated MIBI). **Methods:** We studied 121 patients with a rest gated Tl (3–3.5 mCi, 35 sec/projection)/poststress gated MIBI (25–30 mCi, 25 sec/projection) separate dual-isotope protocol on a 90° dual-detector camera. Automatic quantitation of LVEFs was accomplished using previously developed and validated software, while visual scoring of motion and thickening was performed using four-point scales. **Results:** Average myocardial counts were lower in gated Tl images (306 ± 81 counts/pixel) compared to gated MIBI images (789 ± 237 counts/pixel). The quality of gated Tl images was ranked as excellent, good, fair and poor in 24.0%, 42.1%, 24.8% and 9.1%, respectively, of the patients, compared to 43.0%, 43.8%, 9.1% and 4.1%, respectively, for gated MIBI images. Quantitative-gated Tl and gated MIBI LVEFs correlated well ($y = 0.11+1.05x$, $r = 0.918$, SEE = 6.35). Possible poststress myocardial stunning may have caused gated Tl LVEFs to overestimate gated MIBI LVEFs by a larger ($p = 0.03$) amount in ischemic patients ($n = 47$, $y = -0.69+1.09x$, $r = 0.914$, s.e.e. = 6.44) compared to nonischemic patients ($n = 64$, $y = -1.58+1.05x$, $r = 0.919$, s.e.e. = 5.93), the residual difference in LVEFs for this latter group being likely due to different isotope resolution in conjunction with small left ventricles. Exact agreement between gated Tl and gated MIBI segmental myocardial function in 41 nonischemic patients was 92.2% (kappa = 0.619) and 95.4% (kappa = 0.586) for motion and thickening scores, respectively. **Conclusion:** Thallium-201 gated SPECT imaging can be effectively performed on the majority of patients in our clinical environment and offers the opportunity to assess both myocardial perfusion and function using one injection and one imaging sequence, similarly to what is done with $^{99m}$Tc-based agents.

**Key Words:** gated myocardial perfusion SPECT; thallium-201; automatic quantitative LVEF

**J Nucl Med 1997; 38:749–754**

The introduction of new, $^{99m}$Tc-based myocardial perfusion agents, such as $^{99m}$Tc-sestamibi, has generated a great deal of interest in the performance of gated SPECT perfusion studies (*1–3*). The main benefit of this technique is its ability to provide information on myocardial perfusion and function (motion, thickening, ejection fraction) using one injection and one imaging sequence. In some patient populations, this approach may effectively replace the classical rest/stress technique, with efficiency and cost benefits important in the current health care environment (*4*). In conjunction with the diffusion of $^{99m}$Tc-sestamibi gated SPECT, software and algorithms have been developed that make it easier to measure functional parameters from gated SPECT images (*5,6*). Recently, our laboratory developed and validated an automatic and accurate method to measure left ventricular ejection fraction (LVEF) from $^{99m}$Tc-sestamibi gated SPECT images (*7*). We also successfully applied the same method to low-count images resulting from a standard $^{99m}$Tc-sestamibi injection and a fast (6.7-min) gated SPECT acquisition protocol (*8*), with the ultimate goal of measuring true stress myocardial function using pharmacologic stress and a very short gated-acquisition sequence (*9*). The current study investigates whether myocardial function assessment is applicable to another class of relatively low-count images, those produced by gated $^{201}$Tl perfusion SPECT acquisition (*10,11*).

Despite the increasing diffusion of technetium-based agents, $^{201}$Tl remains the most widely used radioisotope for myocardial perfusion SPECT. About 60% of all cardiac SPECT studies currently performed in the U.S. are performed with $^{201}$Tl. Reasons why $^{201}$Tl is unlikely to be completely replaced by $^{99m}$Tc-based agents include the usefulness of $^{201}$Tl lung uptake in providing a noninvasive assessment of pulmonary wedge pressure, the cost of the radiopharmaceutical and the fact that $^{201}$Tl is still widely considered the agent of choice for myocardial viability assessment with perfusion SPECT. However, artifactual perfusion defects caused by photon attenuation represent an especially critical problem in $^{201}$Tl perfusion SPECT, due to the lower photon energy of $^{201}$Tl compared to $^{99m}$Tc. Gated $^{201}$Tl SPECT studies would allow easier detection of such attenuation artifacts, while potentially providing information on myocardial perfusion and function using one injection and one imaging sequence. The goal of this article is to determine whether it is possible to obtain good quality eight-interval $^{201}$Tl gated SPECT images, and to compare automatic quantitative measurements of LVEF, as well as semiquantitative visual assessment of regional wall motion and wall thickening derived from patients undergoing rest $^{201}$Tl gated SPECT to analogous measurements from poststress eight-interval $^{99m}$Tc-sestamibi gated SPECT images in the same patients.

## MATERIALS AND METHODS

In this prospective study, gated images were acquired from 121 randomly selected clinical patients undergoing a rest $^{201}$Tl/stress $^{99m}$Tc-sestamibi "separate acquisition dual-isotope" gated SPECT protocol (*12*). In this protocol, injection of 3–3.5 mCi of $^{201}$Tl is followed by $^{201}$Tl SPECT imaging, which then is followed by injection of 25–30 mCi $^{99m}$Tc-sestamibi at peak stress and repeated SPECT imaging 15–30 min later (treadmill exercise, 89 patients) or 1 hr later (pharmacologic stress using adenosine, 32 patients). With this approach, $^{201}$Tl images are uncontaminated by $^{99m}$Tc, and $^{99m}$Tc-sestamibi images are only minimally affected by $^{201}$Tl crosstalk (*13*). The clinical characteristics of the patient population are summarized in Table 1.

Received Jul. 8, 1996; revision accepted Sep. 4, 1996.

For correspondence or reprints contact: Guido Germano, PhD, Director, Nuclear Medicine Physics, Cedars-Sinai Medical Center A047 N, 8700 Beverly Blvd., Los Angeles, CA 90048.

**TABLE 1**
Patient Characteristics

| | |
|---|---|
| No. of patients | 121 |
| No. of men | 83 (69%) |
| Age (yr) | 66 ± 12 |
| Weight (lb) | 165 ± 40 |
| History of MI | 22 (18%) |
| History of CABG | 18 (15%) |
| History of PTCA | 25 (21%) |

All patient studies were acquired on a dual-detector camera with the detectors oriented at 90°. The camera used low-energy, high-resolution (LEHR) collimation, step-and-shoot detector rotation, 64 projections over 180° (45° RAO to LPO) and 35 sec ($^{201}$Tl) or 25 sec ($^{99m}$Tc-sestamibi) of data collection per projection, distributed over eight cardiac frames. The acceptance window for cardiac cycle length was set to its maximum value of 100%, resulting in the acceptance of all counts from cardiac cycles with duration within ± 50% of the average, for each individual patient. The projection datasets were prefiltered with a two-dimensional Butterworth filter (order = 5 and critical frequency = 0.25 cycles/pixel for the $^{99m}$Tc-sestamibi images, order = 5 and critical frequency = 0.20 cycles/pixel for the $^{201}$Tl images, pixel size = 0.64 cm), and reconstructed with filtered backprojection (ramp filter) and no attenuation correction. The resulting transaxial image sets were reoriented into $^{201}$Tl and $^{99m}$Tc-sestamibi short-axis sets, to which our automatic LVEF measuring algorithm was applied. The algorithm (*7*) operates in the three-dimensional space. It segments the left ventricle (LV), estimates and displays endocardial and epicardial surfaces for all gating intervals in the cardiac cycle, calculates the relative LV cavity volumes and derives the global LVEF from the end-diastolic and end-systolic volume, all without operator interaction. Contours are generated even in the apparent absence of perfusion by using smoothness, the isocontours of the coordinate system and the geometry of the defect boundaries as constraints. The entire process executes in about 20 sec on a Pegasys MD (ADAC, Milpitas, CA) display workstation, basically a SunSPARC5 computer with no dedicated or proprietary hardware. The software is modular, written in the C language and uses the X-Windows graphical user interface and the OSF-Motif toolkit, making it easily portable within the Unix environment. In our previously published validation studies (*7*), we demonstrated high agreement between rest left ventricular ejection fractions measured automatically from gated $^{99m}$Tc-sestamibi SPECT, and semiautomatically from gated equilibrium blood pool ventriculography and first pass.

To the extent that the poststress heart function is similar to the resting function, similar LVEFs, regional wall motion and wall thickening should be found based on the $^{201}$Tl or $^{99m}$Tc-sestamibi gated images. To evaluate and minimize the effect of possible poststress myocardial stunning, comparison of the automatically measured LVEFs was performed in all 121 patients as well as in two subsamples of 64 nonischemic and 47 ischemic patients. For the purpose of this analysis, a nonischemic patient was defined, based on a 20-segment semiquantitative visual assessment of myocardial perfusion, as one with no or minimal reversible defects, or a summed difference score (SDS) <2 between rest and stress perfusion images (*12*). An ischemic patient was more restrictively defined as having not only an SDS ≥ 2, but also a summed stress score (SSS) ≥4 (*12*). The 10 patients with SDS ≥ 2 and SSS < 4 were assigned neither to the ischemic nor to the nonischemic category.

In addition to ejection fraction measurements from gated short-axis images, projection images were analyzed to measure the different count statistics of $^{201}$Tl and $^{99m}$Tc-sestamibi images. For each $^{201}$Tl or $^{99m}$Tc-sestamibi study, the eight projection sets corresponding to the different phases of the cardiac cycle were first summed together to generate an ungated or summed set. Then, the projection image corresponding to LAO 45° was automatically extracted from each ungated set, based on the information contained in the image file header. Three projection images from either side of LAO 45° were summed to LAO 45° (total = 7 images, over a 21° arc) to improve image statistics, resulting in a LAO 45° ± 10.5° image. The LV was segmented using a previously described algorithm (*14*). In essence, the LAO 45° ± 10.5° image is convolved with a feature detector, the double derivative of a two-dimensional Gaussian with iteratively varied standard deviation. This operation yields several points, candidates to represent the LV center. The image is then processed by template convolution followed by local maxima extraction. Continuous rings of maximal pixels surrounding the candidate points are identified by breadth-first search and iterative directional pixel dilation, and the ring most likely to represent the LV chosen using size, shape and location heuristics (*14*). Having thus segmented the LV, the maximum, total and average myocardial pixel counts were calculated for the $^{201}$Tl and the $^{99m}$Tc-sestamibi image, and compared.

The overall image quality of gated $^{201}$Tl and $^{99m}$Tc-sestamibi SPECT studies was semiquantitatively assessed in all 121 patients by consensus of two expert observers who were blinded to patient name and history, and did not evaluate $^{201}$Tl and $^{99m}$Tc-sestamibi images of the same patient simultaneously or in immediate succession. For this purpose, a four-point scale based on image resolution, contrast, uniformity and statistics (A = excellent, B = good, C = fair, D = poor) was used. Also, semiquantitative visual assessment of regional (segmental) wall motion and wall thickening from gated $^{201}$Tl and $^{99m}$Tc-sestamibi SPECT was performed in two subsamples of 41 nonischemic and 30 ischemic patients, selected to span the widest possible range of LVEF. Visual assessment [automatic analysis of wall motion and wall thickening is under development at our laboratory (*7*)] was based on consensus of two expert observers and used a total of 20 LV segments, including six evenly-spaced segments in each of an apical, midventricular and basal short-axis slice, and two apical segments in a midventricular vertical long-axis slice, as previously described (*12,15,16*). The gated $^{201}$Tl and $^{99m}$Tc-sestamibi SPECT images were read in cinematic mode, using a smoothed cinematic display routine that performed real time three-point temporal interpolation of the images (with kernel weights of 0.5, 1, 0.5) to reduce noise. Wall motion was scored on a four-point scale (0 = normal, 1 = mild hypokinesia, 2 = moderate to severe hypokinesia, 3 = akinesia or dyskinesia) in the 20 segments described above. Wall thickening was also scored on a four-point scale (0 = normal, 1 = mildly impaired, 2 = moderately impaired, 3 = severely impaired to absent thickening) based on the visual assessment of myocardial wall brightening from diastole to systole (*17,18*) in the same 20 segments.

### Statistical Analysis

Proportions and continuous variables were compared using the two-tailed unpaired Student's t-test, with a p value < 0.05 considered statistically significant. The agreement of LVEF measurements derived from $^{201}$Tl and $^{99m}$Tc-sestamibi gated SPECT was assessed using linear regression (Pearson r) and Bland-Altman analysis (*19*). The agreement of segmental functional measurements derived from $^{201}$Tl and $^{99m}$Tc-sestamibi gated SPECT was assessed from 4 × 4 tables using the unweighted kappa statistics, with a p value < 0.05 considered statistically significant. Kappa values < 0.4, between 0.4 and 0.75, and > 0.75 were taken to

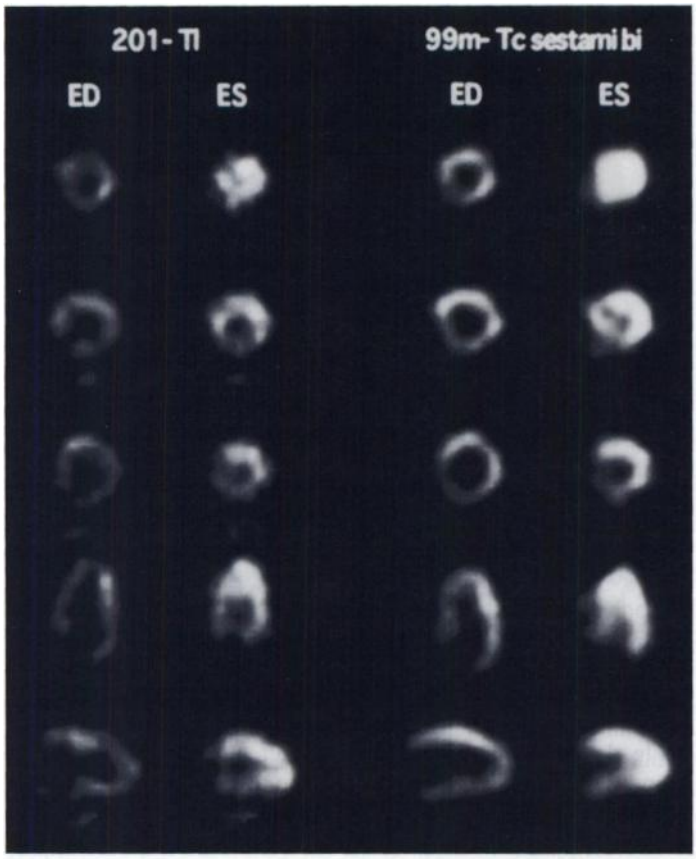


**FIGURE 1.** End-diastolic and end-systolic reoriented tomographic images derived from gated $^{201}$Tl and gated $^{99m}$Tc-sestamibi acquisitions in a normal patient.

represent poor, fair to good, and excellent agreement, respectively, based on Fleiss's classification (*20*).

## RESULTS

Figure 1 shows a synthetic comparison of the image quality of gated $^{201}$Tl versus that of gated $^{99m}$Tc-sestamibi SPECT, in a normal patient. Each column contains three short-axis (top to bottom = apical to basal), a midventricular horizontal and a midventricular vertical long-axis image. The two leftmost columns contain the gated $^{201}$Tl images corresponding to the end-diastolic and end-systolic phase of the cardiac cycle, while the two rightmost columns present the same information for the gated $^{99m}$Tc-sestamibi study. Overall, the reviewing physicians judged the quality of the individual gated $^{201}$Tl and gated $^{99m}$Tc-sestamibi images to be adequate in all 121 patients. Specifically, gated $^{201}$Tl image quality was rated as excellent, good, fair and poor in 29 (24.0%), 51 (42.1%), 30 (24.8%) and 11 (9.1%) patients, respectively. The corresponding values for gated $^{99m}$Tc-sestamibi images were 52 (43.0%), 53 (43.8%), 11 (9.1%) and 5 (4.1%), respectively (Fig. 2). Quantitative measurement of maximum pixel myocardial counts from the 121 patients' LAO 45° ± 10.5° projection images yielded values of 1,183 ± 344 counts for $^{99m}$Tc-sestamibi, and 434 ± 116 counts for $^{201}$Tl. Similarly, average myocardial counts measured from the same images were 789 ± 237 counts/pixel for $^{99m}$Tc-sestamibi, compared to 306 ± 81 counts/pixel for $^{201}$Tl. The ratio of average $^{99m}$Tc-sestamibi to average $^{201}$Tl myocardial counts was 2.66 ± 0.77 over the 121 patients.

The standard output of the automated algorithm for the quantitative measurement of LVEF is shown for the normal patient in Figure 3. Figure 3 displays the same three short-axis, horizontal and vertical long-axis images as in the leftmost column of Figure 1 (normal gated $^{201}$Tl patient at end diastole),

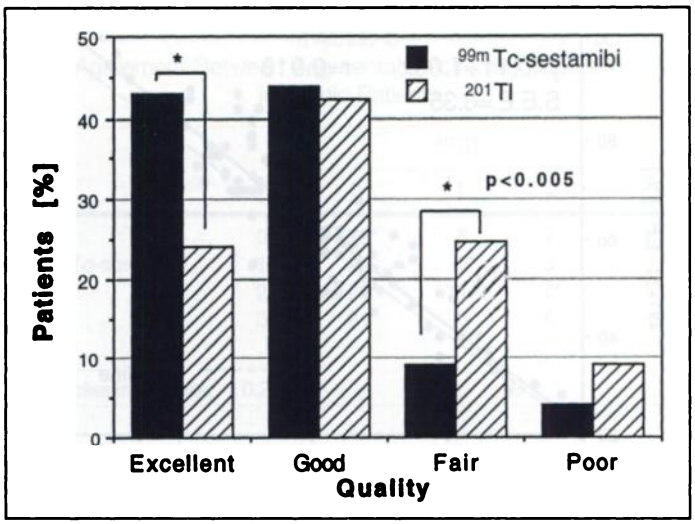


**FIGURE 2.** Comparison of $^{201}$Tl and $^{99m}$Tc-sestamibi gated SPECT image quality in 121 patients.

with endocardial and epicardial contours superimposed onto all images. The software algorithm executed successfully in 235/242 (97.1%) of the studies, with a small, not statistically significant difference between $^{201}$Tl (six failures) and $^{99m}$Tc-sestamibi (one failure). Failure was defined as the generation of endocardial and epicardial contours that did not visually appear to bound the myocardium, and was always due to the presence of substantial hepatic or intestinal uptake in conjunction with low myocardial counting statistics. The software's user interface allows for the manual placement of a three-dimensional ellipsoidal region of interest (ROI) around the myocardium, thus constraining the segmentation and surface detection process to the image portion within the ROI. This approach was applied to the seven cases in which the algorithm failed, always resulting in successful completion of processing. Figure 4 shows the relationship between the ejection fractions measured by our automatic algorithm from the gated $^{201}$Tl and $^{99m}$Tc-sestamibi images, in the 121 patients population. Ejection fractions derived from $^{201}$Tl images are linearly related ($y = 0.11 + 1.05x$) and agree very well ($r = 0.918$, s.e.e. = 6.35) with those derived from $^{99m}$Tc-sestamibi images. There is a slight tendency on the part of $^{201}$Tl measurements to overestimate the ejection fraction compared to $^{99m}$Tc-sestamibi measurements, as demonstrated by the solid regression line being higher than the dashed identity line in Figure 4. It is possible

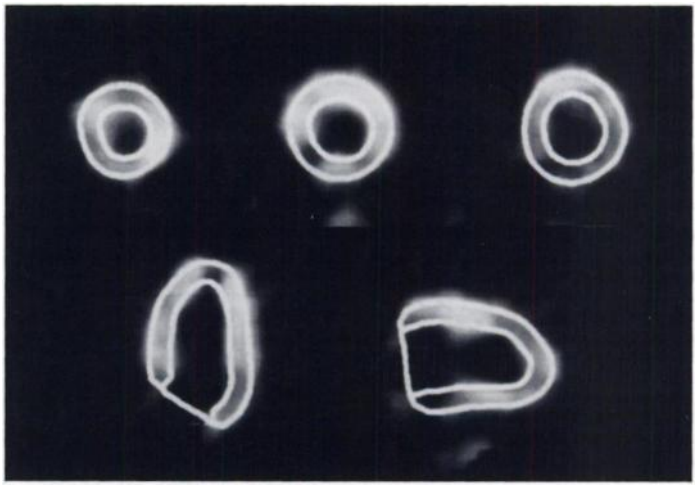

**FIGURE 3.** End-diastolic gated $^{201}$Tl SPECT images for the normal patient in Figure 1, with overlayed endocardial and epicardial contours calculated by the automated algorithm for the quantitative measurement of LVEF.

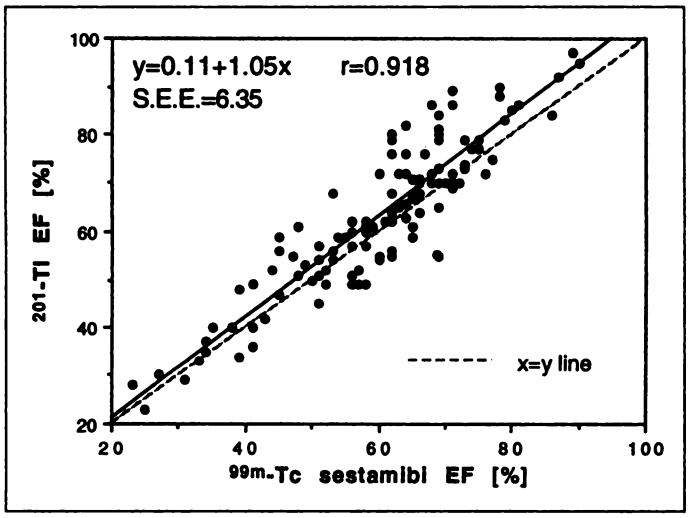


**FIGURE 4.** Comparison of LVEFs automatically derived from $^{201}$Tl and $^{99m}$Tc-sestamibi gated SPECT images of all 121 patients studied.

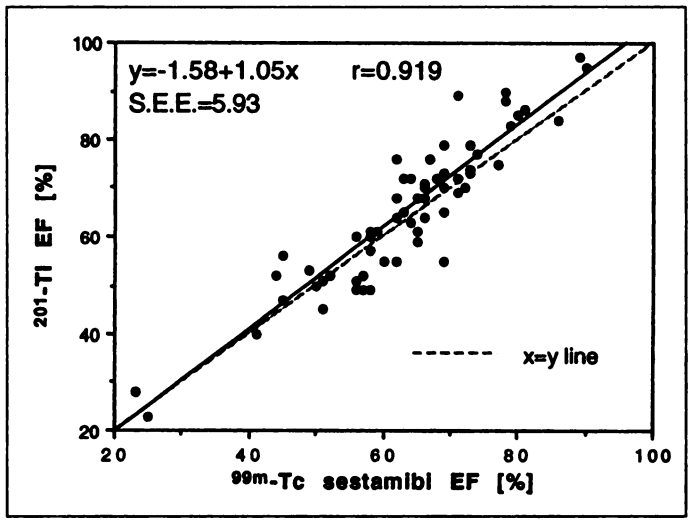


**FIGURE 6.** Comparison of LVEFs automatically derived from $^{201}$Tl and $^{99m}$Tc-sestamibi gated SPECT images of 64 nonischemic patients.

that this tendency is due at least in part to the presence of poststress myocardial stunning in the $^{99m}$Tc-sestamibi images. In fact, if only the 47 ischemic patients (SSS ≥ 4, SDS ≥ 2) are considered (Fig. 5), the $^{201}$Tl LVEFs are even higher compared to the $^{99m}$Tc-sestamibi LVEFs ($y = -0.68 + 1.09x$), and the solid regression line further diverges from the dashed identity line, although the agreement between the two sets of measurements remains very good ($r = 0.914$, s.e.e. = 6.44). As expected, comparing LVEFs from $^{201}$Tl and $^{99m}$Tc-sestamibi images in the 64 nonischemic patients (SDS < 2) results in the best agreement ($y = -1.58 + 1.05x$, $r = 0.919$, SEE = 5.93), and Figure 6 shows that the solid regression line is very close to the dashed identity line for those patients. Bland-Altman type analysis demonstrated a significant difference between the ischemic and the nonischemic subgroup with respect to concordance of LVEF measurements derived from $^{201}$Tl and $^{99m}$Tc-sestamibi gated SPECT images (mean difference of $^{201}$Tl/$^{99m}$Tc LVEF measurements ± s.d. = 4.4 ± 6.5 for ischemic versus 1.8 ± 5.9 for nonischemic patients, $p = 0.03$).

Comparison of visually-assessed $^{201}$Tl and $^{99m}$Tc-sestamibi segmental wall motion and thickening in 41 nonischemic patients also demonstrated good agreement between the two isotopes. In particular, Table 2 shows the relationship between $^{201}$Tl and $^{99m}$Tc-sestamibi segmental motion scores (exact agreement = 92.2%, kappa = 0.619), while Table 3 shows the relationship between segmental thickening scores (exact agreement = 95.4%, kappa = 0.586). In contrast, only poor to fair agreement between $^{201}$Tl and $^{99m}$Tc-sestamibi segmental function was found in 30 ischemic patients, as demonstrated in Table 4 for the motion scores (exact agreement = 78.2%, kappa = 0.471), and in Table 5 for the thickening scores (exact agreement = 80.2%, kappa = 0.214). The disproportionate presence of high motion and thickening scores in the lower left portion of Tables 4 and 5 suggests that poststress myocardial stunning may be present in the $^{99m}$Tc-sestamibi gated SPECT images of some of the visually-assessed ischemic patients.

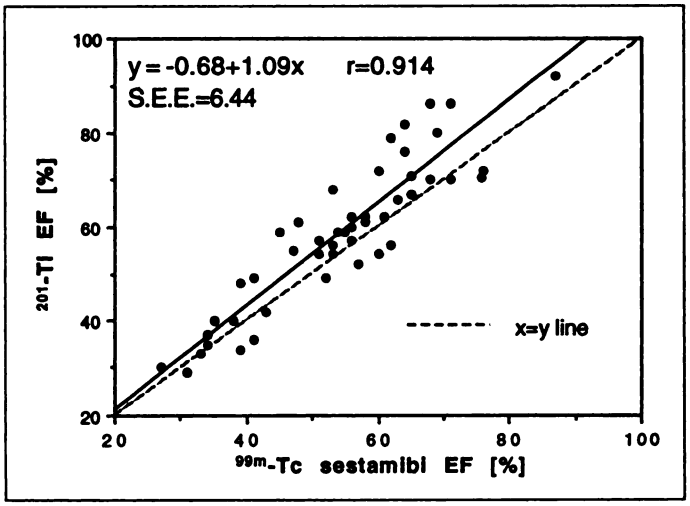


**FIGURE 5.** Comparison of LVEFs automatically derived from $^{201}$Tl and $^{99m}$Tc-sestamibi gated SPECT images of 47 ischemic patients.

## DISCUSSION

This study does not include a straightforward comparison of rest $^{201}$Tl and rest $^{99m}$Tc-sestamibi gated SPECT images, the acquisition of which would have disrupted our clinical operation based on the rest $^{201}$Tl/stress $^{99m}$Tc-sestamibi separate dual-isotope protocol. Our alternative approach was to isolate and evaluate the effect of poststress alteration of myocardial function by dividing our patient population into a definitely ischemic and a nonischemic group based on rest/stress semiquantitative perfusion scores, then performing LVEF, wall motion and wall thickening comparison analyses on both groups. Comparing LVEFs (Fig. 5) and regional function (Tables 4 and 5) from rest $^{201}$Tl and poststress $^{99m}$Tc-sestamibi gated SPECT images in ischemic patients suggests that myocardial stunning can indeed affect global and regional measurements of function. However, a systematic investigation of the effect of myocardial stunning on quantitative LVEFs and semiquantitative segmental myocardial function in a different

**TABLE 2**
Agreement Between Technetium-99m-Sestamibi and Thallium-201 Gated SPECT Segmental Motion Scores in Nonischemic Patients

| | | $^{201}$Tl | | | |
|---|---|---|---|---|---|
| | | 0 | 1 | 2 | 3 |
| $^{99m}$Tc-sestamibi | 0 | 704* | 9 | 9 | 1 |
| | 1 | 21 | 4* | 4 | 0 |
| | 2 | 9 | 4 | 31* | 1 |
| | 3 | 1 | 0 | 5 | 17* |

* Motion (kappa = 0.619).

**TABLE 3**
Agreement Between Technetium-99m-Sestamibi and Thallium-201 Gated SPECT Segmental Thickening Scores in Nonischemic Patients

| | | $^{201}$Tl | | | |
|---|---|---|---|---|---|
| | | 0 | 1 | 2 | 3 |
| $^{99m}$Tc-sestamibi | 0 | 759* | 14 | 4 | 0 |
| | 1 | 3 | 5* | 5 | 0 |
| | 2 | 5 | 2 | 3* | 1 |
| | 3 | 1 | 1 | 2 | 15* |

* Thickening (kappa = 0.586).

patient population is being performed in collaboration with another laboratory (Johnson L, *personal communication*, 1996), and was beyond the scope of this study.

Figure 6 shows that LVEFs are still higher for $^{201}$Tl compared to $^{99m}$Tc-sestamibi images, even if the influence of myocardial stunning is minimized by using data from nonischemic patients alone. This is likely due to the intrinsic difference in image resolution between $^{201}$Tl and $^{99m}$Tc, reduced but not eliminated by the use of low-energy, high-resolution collimators for both acquisitions. The difference in resolution would be expected to create problems in small hearts, where the dual smoothing introduced by prereconstruction filtering and tomographic reorientation may cause the apparent disappearance of the LV cavity in the end-diastolic $^{201}$Tl images, and the consequent overestimation of the $^{201}$Tl LVEF. Figure 6 supports this hypothesis, as the solid regression line and the dashed identity line diverge most markedly at high ejection fractions, typically corresponding to smaller LV cavity volumes. It should be noted, however, that this small artifactual increase in $^{201}$Tl LVEFs for LVEFs > 60 is likely not clinically significant. In future perspective, we plan to increase pixel sampling of the LV cavity in the short-axis images by implementing zoomed off-axis reconstruction, both for gated and nongated SPECT applications. This approach can reduce pixel size by more than 50% compared to standard reconstruction, and is expected to further reduce isotope-related differences in volume estimates of small LV cavities. In fact, isotope-dependent differences in LV cavity volume measurements were less pronounced in our previously reported work using a camera that allowed for zoomed on-axis reconstruction (*21*). In that study, automatically derived LV cavity volumes from $^{99m}$Tc-sestamibi and $^{201}$Tl perfusion SPECT images of 54 normal patients were found to be, on average, within 2%–3% of each other, and their ratio helped establish normal limits for transient ischemic dilation, a marker of severe and extensive coronary artery disease (*21,22*).

**TABLE 4**
Agreement Between Technetium-99m-Sestamibi and Thallium-201 Gated SPECT Segmental Thickening Scores in Ischemic Patients

| | | $^{201}$Tl | | | |
|---|---|---|---|---|---|
| | | 0 | 1 | 2 | 3 |
| $^{99m}$Tc-sestamibi | 0 | 408* | 4 | 7 | 0 |
| | 1 | 26 | 2* | 6 | 0 |
| | 2 | 41 | 19 | 49* | 3 |
| | 3 | 6 | 1 | 18 | 10* |

* Motion (kappa = 0.471).

**TABLE 5**
Agreement Between Segmental Thickening Scores in Ischemic Patients

| | | $^{201}$Tl | | | |
|---|---|---|---|---|---|
| | | 0 | 1 | 2 | 3 |
| $^{99m}$Tc-sestamibi | 0 | 473* | 8 | 7 | 2 |
| | 1 | 24 | 3* | 3 | 0 |
| | 2 | 28 | 11 | 2* | 1 |
| | 3 | 21 | 8 | 6 | 3* |

* Thickening (kappa = 0.214).

## CONCLUSION

To achieve an accurate and reproducible comparison of $^{99m}$Tc-sestamibi and $^{201}$Tl perfusion gated SPECT, we believe that regional measurements of wall motion and wall thickening should be quantitative and fully automatic. We are investigating and developing techniques that will allow automatic quantitation of regional function from gated SPECT data, generation of normal limits for myocardial wall motion and thickening, and combination of perfusion and function information in parametric polar map format.

## ACKNOWLEDGMENTS

We thank John Friedman, MD and Mark Hyun, CNMT for their assistance. This work was supported in part by a Whitaker Foundation Biomedical Engineering Research Grant.

## REFERENCES

1. Mannting F, Morgan-Mannting M. Gated SPECT with technetium-99m-sestamibi for assessment of myocardial perfusion abnormalities. *J Nucl Med* 1993;34:601–608.
2. Grucker D, Florentz P, Ozwald T, Chambron J. Myocardial gated tomo-scintigraphy with $^{99m}$Tc-methoxy-isobutyl-isonitrile (MIBI): regional and temporal activity curve analysis. *Nucl Med Commun* 1989;10:723–732.
3. Berman D, Kiat H, Van Train K, Germano G, Maddahi J, Friedman J. Myocardial perfusion imaging with technetium-99m-sestamibi: comparative analysis of available imaging protocols. *J Nucl Med* 1994;35:681–688.
4. Chua T, Kiat H, Germano G, et al. Gated technetium-99m-sestamibi for simultaneous assessment of stress myocardial perfusion, post-exercise regional ventricular function and myocardial viability: correlation with echocardiography and rest thallium-201 scintigraphy. *J Am Coll Cardiol* 1994;23:1107–1114.
5. Faber T, Stokely E, Peshock R, Corbett J. A model-based four-dimensional left ventricular surface detector. *IEEE Trans Med Imag* 1991;10:321–329.
6. DePuey E, Nichols K, Dobrinsky C. Left ventricular ejection fraction assessed from gated technetium-99m-sestamibi SPECT. *J Nucl Med* 1993;34:1871–1876.
7. Germano G, Kiat H, Kavanagh P, et al. Automatic quantification of ejection fraction from gated myocardial perfusion SPECT. *J Nucl Med* 1995;36:2138–2147.
8. Mazzanti M, Germano G, Kiat H, Friedman J, Berman D. Fast technetium-99m-labeled-sestamibi gated single-photon emission computed tomography for evaluation of myocardial function. *J Nucl Cardiol* 1996;3:143–149.
9. Germano G, Kiat H, Mazzanti M, Friedman J, Berman D. Stress perfusion/stress wall motion with fast (6.7 min) technetium-sestamibi gated myocardial SPECT [Abstract]. *J Nucl Med* 1994;35:81P.
10. Mochizuki T, Murase K, Fujiwara Y, Tanada S, Hamamoto K, Newlon Tauxe W. Assessment of systolic thickening with thallium-201 ECG-gated single-photon emission computed tomography: a parameter for local left ventricular function. *J Nucl Med* 1991;32:1496–1500.
11. Mochizuki T, Murase K, Fujihara Y, et al. ECG-gated thallium-201 myocardial SPECT in patients with old myocardial infarction compared with ECG-gated blood pool SPECT. *Ann Nuklearmedizin* 1991;5:47–51.
12. Berman D, Kiat H, Friedman J, et al. Separate acquisition rest thallium-201/stress technetium-99m sestamibi dual isotope myocardial perfusion SPECT: a clinical validation study. *J Am Coll Cardiol* 1993;22:1455–1464.
13. Kiat H, Germano G, Friedman J, et al. Comparative feasibility of separate or simultaneous rest thallium-201/stress technetium-99m-sestamibi dual-isotope myocardial perfusion SPECT. *J Nucl Med* 1994;35:542–548.
14. Germano G, Kavanagh P, Chen J, et al. Operator-less processing of myocardial perfusion SPECT studies. *J Nucl Med* 1995;36:2127–2132.
15. Kiat H, Berman D, Maddahi J. Late reversibility of tomographic myocardial thallium-201 defects: an accurate marker of myocardial reversibility. *J Am Coll Cardiol* 1988;12:1456–1463.
16. Yang L, Berman D, Kiat H, et al. The frequency of late reversibility in SPECT thallium-201 stress-redistribution studies. *J Am Coll Cardiol* 1990;15:334–340.
17. Sorenson J, Phelps M. *Physics in nuclear medicine*, 2nd ed. Orlando, FL: Grune and Stratton; 1987.

18. Cooke C, Garcia E, Cullom S, Faber T, Pettigrew R. Determining the accuracy of calculating systolic wall thickening using a fast Fourier transform approximation: a simulation study based on canine and patient data. *J Nucl Med* 1994;35:1185–1192.
19. Bland J, Altman D. Statistical methods for assessing agreement between two methods of clinical measurement. *Lancet* 1986;1:307–310.
20. Fleiss J. *Statistical methods for rates and proportions*, 2nd ed. New York, NY: Wiley; 1981.
21. Mazzanti M, Germano G, Kiat H, et al. Identification of severe and extensive coronary artery disease by automatic measurement of transient ischemic dilation of the left ventricle in dual-isotope myocardial perfusion SPECT. *J Am Coll Cardiol* 1996;27:1612–1620.
22. Weiss A, Berman D, Lew A, et al. Transient ischemic dilation of the left ventricle on stress thallium-201 scintigraphy: a marker of severe and extensive coronary artery disease. *J Am Coll Cardiol* 1987;9:752–759.

# Comparison of SPECT and Ectomography for Evaluating Myocardial Perfusion with Technetium-99m-Sestamibi

Susanne M. Dale, Dianna E. Bone, Lars-Åke Brodin and Catharina Lindström
*Department of Medical Laboratory Sciences and Technology, Division of Medical Engineering, Karolinska Institute; Department of Clinical Physiology, Thoracic Clinics, Karolinska Hospital, Huddinge, Sweden*

This study compared myocardial perfusion scintigraphy performed with ectomography to corresponding SPECT studies. **Methods:** In a comparative study between SPECT and ectomography, 19 patients with suspected coronary artery disease were imaged under similar conditions. A two-day protocol using $^{99m}$Tc-sestamibi was followed. In SPECT, 32 projection images were acquired by rotating the gamma camera detector through 180°, from 45° left posterior oblique to 45° right anterior oblique. Short-axis view sections and polar tomograms were reconstructed. In ectomography, a 30° slant-hole collimator was rotated through 360° in front of a stationary detector to obtain 64 projection images with different projection directions. The gamma camera was orientated perpendicular to the long axis of the left ventricle; the orientation was determined from the SPECT examination. Short-axis section images through the projected conical volume were reconstructed using a two-dimensional filtered back projection technique. In a blind test, the relative diagnostic value and image quality of the two methods were evaluated by three independent observers assessing short-axis view sections and polar tomograms. An objective evaluation based on relative values in the polar tomograms was also performed. The interpretations were evaluated with analysis of variance. **Results:** After injection during exercise, there was no significant difference between SPECT and ectomography. After injection at rest, visualization of the left ventricle was superior ($p < 0.05$) and influence of external activity was less ($p < 0.005$) in ectomography. The activity level within a perfusion defect was significantly lower ($p < 0.05$) and its extension significantly larger ($p < 0.05$) in ectomography than in SPECT. There was no difference between the diagnosis based on SPECT or ectomography. **Conclusion:** In myocardial perfusion imaging with $^{99m}$Tc-sestamibi, ectomography provides information similar to that obtained with SPECT and can, therefore, be used clinically for evaluation of myocardial perfusion when the gamma camera is postitioned perpendicular to the long axis of the left ventricle.

**Key Words:** coronary artery disease; myocardial perfusion; SPECT; technetium-99m-sestamibi; ectomography

**J Nucl Med 1997; 38:754–759**

Myocardial perfusion imaging for diagnosis of coronary artery disease is generally performed using SPECT. A gamma camera detector is rotated around the long axis of the patient, consequently a SPECT system is heavy and stationary. The distance to the object imaged is, for most projection images, rather large, reducing resolution and increasing the attenuation effects. Since a patient must be transported to the camera and is required to lie on a narrow examination table, it is difficult or impossible to perform examinations on critically ill patients connected to life support equipment, such as a ventilator, aortic balloon pump or extra corporeal membrane oxygenation (ECMO) machine. Furthermore, it has been shown that myocardial perfusion scintigraphy provides both diagnostic and prognostic information in patients with suspected acute myocardial infarction (*1–5*). It would, therefore, assist in patient management if such studies could be performed at the bedside, or in the emergency room on patients presenting chest pain.

A tomographic method called ectomography has been developed and implemented in gamma camera imaging (*6*). Ectomography is a limited-view angle method and a set of projection images can be obtained by rotating a slant-hole collimator in front of a stationary gamma camera detector. No complex, heavy gantry for the rotation of the camera is required, making the technique suitable for implementation in a mobile system. Mobility provides the possibility of tomographic imaging in almost all hospital environments, for example in the intensive care unit, emergency room or in the operating theater. Since no active patient cooperation is required, both seriously ill and unconscious patients can be studied. Another advantage of the technique is that the detector can be positioned close to the object during the acquisition of all projection images, thus increasing resolution and reducing attenuation effects. All limited-view angle methods are characterized, however, by an incomplete dataset. For ectomography, this leads to a reduction in depth resolution, which is inversely dependant on view angle (*7*). With the current reconstruction technique, only slices perpendicular to the axis of rotation are tenable. In an extended object, this effect can be minimized by positioning the long axis of the object along the axis about which the collimator rotates (alt axis of rotation). Thus, when imaging the left ventricle, short-axis view slices are obtained when positioning is optimized.

Ectomography has previously been evaluated by computer simulations, phantom studies and a limited number of clinical examinations (*8–9*). A first prototype mobile system was designed and built in our department and is currently at the Department of Clinical Physiology, Thoracic Clinics, Karolinska Hospital, for preliminary clinical evaluation (*10–12*).

This is a comparative study between SPECT and ectomography to verify the clinical accuracy of ectomography for myocardial perfusion imaging using $^{99m}$Tc-sestamibi under ideal geometrical conditions. Thus, to avoid the possible effects

Received Apr. 1, 1996; revision accepted Oct. 2, 1996.
For correspondence or reprints contact: Susanne Dale, PhD, Division of Medical Engineering, F60, Novum, S-141 86 Huddinge, Sweden.